Macromolecules
ARTICLE

Macromolecules **2010**, *43*, 9039–9048 **9039**
DOI: 10.1021/ma100783y

Phase Behavior of Neat Triblock Copolymers and Copolymer/Homopolymer Blends Near Network Phase Windows

Maëva S. Tureau,[†] Lixia Rong,[‡] Benjamin S. Hsiao,[‡] and Thomas H. Epps III*,[†]

[†]*Department of Chemical Engineering, University of Delaware, Newark, Delaware 19716, United States, and* [‡]*Department of Chemistry, Stony Brook University, Stony Brook, New York 11974, United States*

Received April 10, 2010; Revised Manuscript Received July 30, 2010

ABSTRACT: The phase behavior of poly(isoprene-*b*-styrene-*b*-methyl methacrylate) (ISM) copolymers near the styrene-rich network phase window was examined through the use of neat triblock copolymers and copolymer/homopolymer blends. Both end-block and middle-block blending protocols were employed using poly(isoprene) (PI), poly(methyl methacrylate) (PMMA), and poly(styrene) (PS) homopolymers. Blended specimens exhibited phase transformations to well-ordered nanostructures (at homopolymer loadings up to 26 vol % of the total blend volume). Morphological consistency between neat and blended specimens was established at various locations in the ISM phase space. Copolymer/homopolymer blending permitted the refinement of lamellar, hexagonally packed cylinder, and disordered melt phase boundaries as well as the identification of double gyroid (Q^{230}), alternating gyroid (Q^{214}), and orthorhombic (O^{70}) network regimes. Additionally, the experimental phase diagram exhibited similar trends to those found in a theoretical ABC triblock copolymer phase diagram with symmetric interactions and statistical segments lengths generated by Tyler et al.

Introduction

The self-assembly of block copolymers on the nanometer length scale has motivated extensive research efforts in the polymer community over the past several decades. Block copolymer phase separation into ordered nanostructures is driven by the competing effects of block incompatibility and conformational entropy of the polymer chains.[1] Unlike numerous reported 1-D and 2-D block copolymer morphologies that require alignment techniques for optimal transport,[2−4] triply periodic network structures possess continuously, percolating domains in three dimensions. This attribute potentially provides nanostructured polymeric materials with a combination of long-range translational order and mechanical properties that could be useful in commercial applications, including nanotemplating, membrane separations, and ion-conduction.[5]

AB diblock copolymers are characterized by two major parameters: the component volume fraction (f_A), where $f_B = 1 - f_A$, and the segregation strength ($\chi_{AB}N$), which is the product of the segment−segment interaction parameter (χ_{AB}) and the degree of polymerization (N). Whereas AB diblocks exhibit spherical (S), cylindrical (HEX), and lamellar (LAM) morphologies over the vast majority of compositions, the double gyroid network structure (Q^{230}) is identified in a relatively narrow composition window.[6,7]

The addition of a third block, to form ABC triblock copolymers, leads to increased morphological complexity due to the introduction of additional tunable parameters, including three χ parameters (χ_{AB}, χ_{BC}, and χ_{AC}), two independent volume fractions (f_A and f_B, where $f_C = 1 - f_A - f_B$), and the overall degree of polymerization (N). In ABC triblock melts, numerous complex morphologies have been reported,[6] including two- and three-domain LAM morphologies,[8−15] core−shell versions of HEX and S,[8−11,15−17] three equilibrium network phases (core−shell gyroid Q^{230}, alternating gyroid Q^{214}, and orthorhombic O^{70}),[8,9,12,13,18−21] and other mixed-phase morphologies.[11,22] ABC network structures appear to be favored in nonfrustrated polymeric systems that obey the χ-parameter sequence: $\chi_{AC} > \chi_{BC} \geq \chi_{AB}$, where the most incompatible block interaction A/C is not forced by block connectivity.[23] Several nonfrustrated ABC copolymer systems have led to the discovery of network structures in literature.[9,10,12−16,18,20,21] However, only a handful of these nonfrustrated systems allow us to define the extent of the network phase boundaries to make them readily accessible on the commercial scale.[12,15,21]

Exploring the phase behavior and network phase boundaries in ABC systems requires intensive synthesis and characterization efforts. Blending block copolymers with judicious constituent homopolymers has proven to be an effective and economical means to probe the general behavior of neat block copolymers containing comparable composition and segregation strength.[21,24−32] However, it should be noted that in some cases copolymer/homopolymer blend morphologies are not identical to the morphologies of the neat materials at equivalent compositions.[21] Additionally, copolymer blends have exhibited morphologies not found in neat materials,[33−35] in particular, through stabilization of cocontinuous structures.[36] A random phase approximation prediction by Bosse et al. also showed that addition of A-attractive C homopolymer to AB diblock copolymers can significantly alter the blend phase behavior by tuning the effective copolymer segregation strength.[37]

According to studies by Hashimoto et al. and Winey et al.,[38−41] three main blending regimes govern the phase behavior of AB diblock/A homopolymer blends. (1) In the "wet brush" regime ($M_{n_{A,h}}/M_{n_{A,b}} < 1$), the homopolymer A is uniformly distributed within the corresponding A domain and swells block A in the copolymer. (2) In the intermediate "dry brush" regime ($M_{n_{A,h}}/M_{n_{A,b}} \approx 1$), the homopolymer A is locally solubilized in the center of the corresponding block domain without significant swelling. (3) Finally, blends for which $M_{n_{A,h}}/M_{n_{A,b}} \gg 1$ lead to macrophase

*To whom correspondence should be addressed. E-mail: thepps@udel.edu. Fax: (302) 831-3009.

Published on Web 10/07/2010

separation.[1] Therefore, the homopolymer should be the minority component in the polymer blend (generally $f_h < 0.30$), and the homopolymer molecular weight ($M_{n_{A,h}}$) should be roughly less than or equal to the corresponding block molecular weight ($M_{n_{A,b}}$) to avoid macrophase separation and minimal morphological differences between blended and neat materials.[1,21,32] We expect ABC triblock−homopolymer blends to follow the similar mixing patterns. However, we note that the midblock B of an ABC triblock has a bridge conformation, and addition of B homopolymer will force the B chains of the copolymer to stretch, whereas the addition of A or C homopolymers to an ABC triblock copolymer does not necessarily require the corresponding A and C chains to elongate, thus complicating the phase behavior.[1,26]

To the best of our knowledge, the poly(isoprene-*b*-styrene-*b*-ethylene oxide) (ISO) system is the only experimental system in which the comprehensive network phase locations were investigated at weak-to-intermediate segregation strengths in both neat and blended materials.[12−15,21,42] The comprehensive neat ISO phase map shows a qualitative match with an asymmetric theoretical ISO phase portrait by Tyler et al. that incorporates experimentally measured χ parameters and block statistical segment lengths into self-consistent field theory (SCFT) calculations.[42] In a recent follow-up publication, Qin et al. provided further analysis of the phase behavior in nonfrustrated symmetric ABC and asymmetric ISO triblock systems.[43]

In this work, we utilize poly(isoprene-*b*-styrene-*b*-methyl methacrylate) (ISM) triblock copolymers, a nonfrustrated and nearly symmetric polymeric system with statistical segment length ratios close to unity ($b_M/b_I = 0.95$, $b_I/b_S = 1.11$, $b_S/b_M = 0.95$),[44] and a χ-parameters sequence: χ_{IM}[45] $\gg \chi_{IS}$[46] $\geq \chi_{SM}$.[47] Therefore, our nearly ideal ISM system provides an experimental framework that can be directly compared with a symmetric model ABC phase diagram by Tyler et al.[42] Additionally, the ISM system was chosen for the toughness provided by the combined poly(isoprene)/poly(styrene) (PI/PS) block interactions, the mechanical strength given by the PS domain, and the ease of removal of the poly(methyl methacrylate) (PMMA) block through etching to produce nanoporous templates.

In a previous publication, we reported the characterization of six ISM triblock copolymers that exhibited various morphologies including the Q^{214} network phase in the weak-to-intermediate segregation regimes.[48] Our objective in this work is to extend the exploration of the ISM network phases and refine the network phase boundaries by inducing phase transformations via the blending of ISM neat triblocks with PI, PS, and PMMA homopolymers. The blend phase behavior is found to match closely the behavior of neat ISM triblocks of comparable compositions and segregation strengths, whereas the morphological consistency between blends is verified from two blends of comparable composition obtained from two different parent triblock copolymers. Additionally, the estimated ISM phase map of neat and blended specimens in the network-rich windows matches the general behavior predicted by the neat ABC model phase diagram by Tyler et al.[42] These findings demonstrate that appropriate ISM triblock/homopolymer blending can help identify and refine the network phase windows in the styrene-rich region of the ISM phase portrait.

Experimental Section

Material Synthesis. ISM triblock copolymers were synthesized by sequential anionic polymerization of purified isoprene, styrene, and methyl methacrylate monomers. The detailed synthetic procedure is provided elsewhere.[48] PS, hydroxyl-terminated PS, PI, and PMMA homopolymers were synthesized via conventional anionic polymerization techniques using a 1.3 M *sec*-butyllithium initiator. Styrene and isoprene monomers were polymerized at 40 °C in cyclohexane, and methyl methacrylate was polymerized at −78 °C in tetrahydrofuran (THF).[49,50] All polymerizations were conducted for 8 h and were terminated with acidic methanol. The hydroxyl-terminated PS homopolymer was synthesized in the same manner as the PS homopolymer, except it was capped with an ethylene oxide repeat unit and terminated using acidic methanol.[51]

Table 1. ISM Triblock Copolymer Characterization Data

polymer	M_n (g/mol)	PDI	f_I	f_S	f_M	phase
T1	13 500	1.08	0.35	0.46	0.19	LAM
T2	26 700	1.06	0.48	0.40	0.12	LAM
T3	21 600	1.07	0.39	0.55	0.06	LAM
T4	28 100	1.07	0.13	0.44	0.43	LAM
T5	19 500	1.09	0.29	0.51	0.20	Q^{214}
T6	30 900	1.04	0.29	0.67	0.04	HEX
T7	20 500	1.08	0.16	0.57	0.27	DIS

Table 2. Homopolymer Characterization Data

polymer[a]	M_n (g/mol)	PDI
$PMMA_{11k}$	11 300	1.30
$PMMA_{6k}$	6000	1.13
$PMMA_{3k}$	3000	1.27
$PMMA_{1k}$[b]	1100	1.07
PS_{17k}[b]	17 000	1.03
PS_{14k}	13 700	1.06
$PS{-}OH_{9k}$	9100	1.12
PI_{3k}	3400	1.13

[a] Homopolymer names are assigned according to molecular weight. [b] These homopolymers were obtained from Polymer Source.

Blend Preparation. ISM triblock/homopolymer blends were prepared with up to 26 vol % homopolymer content. Precise amounts (by weight) of homopolymer and neat triblock material (generally ∼0.5 g total) were dissolved in 10 mL of methylene chloride. Sample solutions were allowed to stir for a minimum of 12 h and were thoroughly vacuum-dried. (Drying was monitored by disappearance of solvent peak in ^{1}H NMR spectra.)

Chemical Characterization. Molecular weights and polydispersity indices (PDIs) were determined by gel permeation chromatography (GPC) using PS standards with THF as the mobile phase. The GPC system was equipped with a Waters Alliance 2414 refractive index detector and Waters Styragel HR1 and HR4 columns (7.8 × 300 mm each) in series. Copolymer compositions were measured using a Bruker AV-400 ^{1}H NMR spectrometer. Component volume fractions, f_i, were calculated from integrated ^{1}H NMR peak intensities and homopolymer densities at 140 °C ($\rho_{PI} = 0.83$ g/mL, $\rho_{PS} = 0.969$ g/mL, $\rho_{PMMA} = 1.13$ g/mL).[44] Molecular characterization data for the neat triblock copolymers and homopolymers are listed in Tables 1 and 2, respectively. Blend data are located in Table 3.

Small-Angle X-ray Scattering. Small-angle X-ray scattering (SAXS) data were acquired in the Department of Chemical Engineering at the University of Delaware. The Rigaku SAXS instrument contained a 2 kW sealed-tube generator (Cu Kα, 1.54 Å) with a 2 m sample-to-detector distance. SAXS data were collected at 25 °C and plotted as azimuthally averaged scattering intensity versus scattering vector modulus, $q = 4\pi\lambda^{-1}\sin(\theta/2)$, where θ is the scattering angle. These data are referred to as "UD-SAXS data".

Synchrotron SAXS experiments were conducted on the DND-CAT beamline at the Argonne National Laboratory (Advanced Photon Source (APS)). Three setups were used with an incident beam of wavelength $\lambda = 0.827$ Å and Mar CCD detector at a sample-to-detector distance of 4.6 m (and 3.5 or 5.1 m at $\lambda = 0.729$ Å). SAXS experiments were also performed on the X27C beamline at the Brookhaven National Laboratory (National Synchrotron Light Source (NSLS)) using an incident beam of wavelength $\lambda = 1.371$ Å. The scattered radiation was

Table 3. Triblock/Homopolymer Blends Characterization Data

polymer blend	parent triblock[a]	homopolymer type	homopolymer f_h[b]	blend composition f_I	f_S	f_M	phase
B1	T5	$PMMA_{6k}$	0.03	0.27	0.50	0.23	Q^{214}
B2	T5	$PMMA_{6k}$	0.08	0.26	0.47	0.27	Q^{214}
B3	T5	$PMMA_{6k}$	0.12	0.23	0.47	0.30	LAM
B4	T5	$PMMA_{6k}$	0.20	0.22	0.42	0.36	LAM
B5	T5	$PS-OH_{9k}$	0.03	0.27	0.53	0.20	Q^{214}
B6	T5	$PS-OH_{9k}$	0.09	0.26	0.55	0.19	DIS
B7	T5	$PS-OH_{9k}$	0.12	0.25	0.57	0.18	DIS
B8	T5	$PS-OH_{9k}$	0.18	0.23	0.60	0.17	DIS
B9	T5	$PS-OH_{9k}$	0.24	0.21	0.63	0.16	DIS
B10	T5	$PMMA_{6k}$ /$PS-OH_{9k}$	0.19	0.24	0.47	0.29	LAM
B11	T3	$PS-OH_{9k}$	0.05	0.36	0.58	0.06	LAM
B12	T3	$PS-OH_{9k}$	0.08	0.35	0.59	0.06	LAM
B13	T3	$PS-OH_{9k}$	0.12	0.33	0.62	0.05	Q^{230}
B14	T3	$PS-OH_{9k}$	0.16	0.32	0.63	0.05	Q^{230}
B15	T3	$PS-OH_{9k}$	0.21	0.30	0.65	0.05	HEX
B16	T3	$PMMA_{3k}$	0.04	0.36	0.54	0.10	LAM
B17	T6	PI_{3k}	0.06	0.33	0.63	0.04	Q^{230}
B18	T6	$PMMA_{1k}$	0.03	0.28	0.65	0.07	HEX
B19	T6	$PMMA_{1k}$	0.04	0.28	0.64	0.08	HEX
B20	T6	$PMMA_{1k}$	0.05	0.27	0.64	0.09	HEX
B21	T6	$PMMA_{1k}$	0.06	0.27	0.63	0.10	HEX
B22	T6	$PMMA_{1k}$	0.10	0.26	0.60	0.14	HEX
B23	T6	PS_{17k}	0.10	0.26	0.70	0.04	HEX
B24	T6	PS_{17k}	0.26	0.21	0.76	0.03	HEX
B25	T4	PS_{14k}	0.09	0.12	0.49	0.39	LAM
B26	T4	PS_{14k}	0.13	0.11	0.51	0.38	LAM
B27	T4	PS_{14k}	0.25	0.10	0.58	0.32	Q^{230}
B28	T4	$PMMA_{11k}$	0.06	0.12	0.41	0.47	LAM
B29	T4	$PMMA_{11k}$	0.10	0.12	0.39	0.49	LAM
B30	T4	$PMMA_{11k}$	0.20	0.11	0.35	0.54	O^{70}
B31	T4	$PMMA_{11k}$	0.23	0.10	0.34	0.56	O^{70}

[a] Parent triblocks are the neat triblock material used for blending. See Table 1 for parent triblock data. [b] Homopolymer volume fraction, f_h, is calculated from the ratio of the homopolymer volume to the total blend volume. See Table 2 for homopolymer data.

collected on an image plate detector or a Mar CCD detector at a sample-to-detector distance of 1.9 m. Synchrotron SAXS data from the APS and NSLS facilities are referred to as "APS-SAXS" and "NSLS-SAXS" data, respectively.

SAXS samples were thermally annealed under vacuum and then cooled to 25 °C in a chamber equipped with a Linkam THMS600 stage (at the University of Delaware) prior to data acquisition. All SAXS patterns presented in this work are shifted vertically for clarity. Details of the thermal annealing conditions for each sample are reported in the Supporting Information (Table S1).

Transmission Electron Microscopy. Transmission electron microscopy (TEM) micrographs were acquired on a JEOL JEM-2000FX electron microscope operating at 200 kV, except for samples B11, B13, and B15, which were imaged on a Tecnai-12 instrument operating at 120 kV. Annealed samples from SAXS specimens were cut on a Leica Reichart Ultracut cryo-microtome (−60 to −75 °C) using a Diatome diamond knife. The sliced specimens were placed on 400 mesh copper grids and exposed to vapors of a 4% aqueous OsO_4 solution for 10−15 min to enhance the electron contrast between the I-domain (dark) and the S- and M-domains (light).

Results

In this study, we present 7 neat ISM triblock copolymers (Table 1) and 31 associated ISM triblock/homopolymer blends (Table 3) located on a ternary phase map (Figure 1) near the styrene-rich network phase window. Each phase assignment is color-coded; the seven symbols with black outlines indicate the neat ISM materials, whereas the remaining symbols correspond to the ISM blended specimens. Phase boundaries are estimated on the basis of the general trends depicted by the neat and blended specimens, and the boundaries are also guided by theoretical

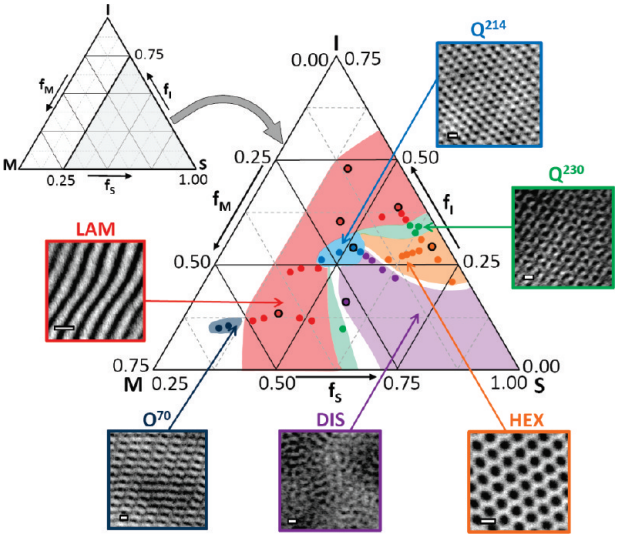

Figure 1. Ternary phase portrait for the poly(isoprene-*b*-styrene-*b*-methyl methacrylate) (ISM) system near the styrene-rich composition window at 25 °C. The axes correspond to the component volume fractions, f_i (where i = I, S, or M). Six microstructures (LAM, Q^{214}, Q^{230}, O^{70}, HEX, and DIS) have been identified in neat (colored circles with black outline) and blended specimens (colored circles). Estimated phase boundaries are represented by color-coded regions and are paired with corresponding TEM micrographs. TEM scale bars represent 20 nm.

predictions from the ABC phase diagram by Tyler et al.[42] and the AB diblock phase diagram by Matsen et al.[7] It should be noted that the lamellar (LAM) phase region in Figure 1 is expected to extend further into the center of the phase diagram according to Tyler's phase diagram; however, the investigation of the S-lean

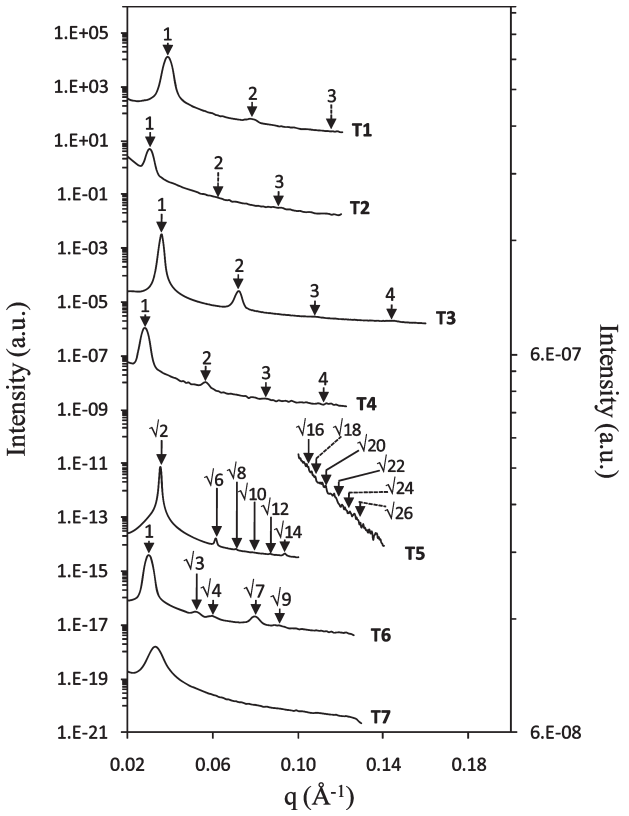

Figure 2. SAXS data for neat ISM triblock copolymers acquired at 25 °C. From top to bottom: SAXS patterns for samples T1, T2, T3, and T4 show Bragg peaks at integral spacings, characteristic of LAM. Diffraction peaks for specimen T5 are indexed according to the $I4_132$ space group, characteristic of the alternating gyroid (Q^{214}) morphology, where the higher-order data are represented on a secondary axis for clarity. The SAXS pattern for sample T6 is indexed according to hexagonal symmetry (hexagonally packed cylinders based on TEM). SAXS data for sample T7 show a broad primary peak at all temperatures, which is suggestive of a disordered (DIS) morphology.

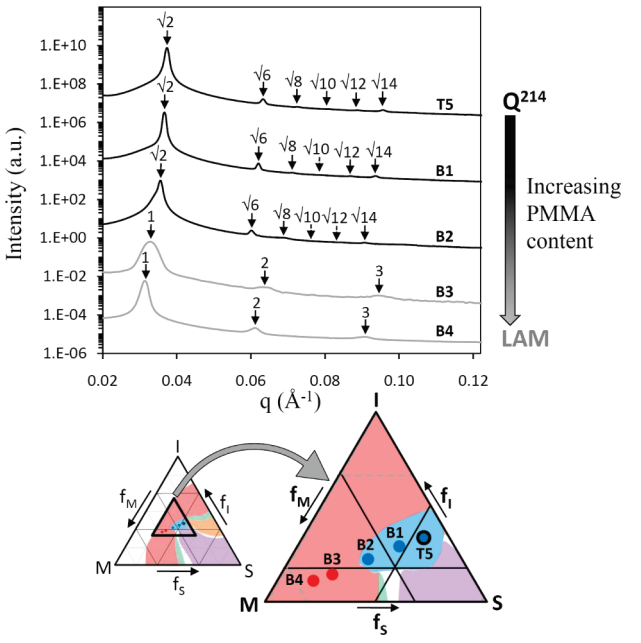

Figure 3. SAXS data for ISM triblock/PMMA homopolymer specimens. From top to bottom: the neat ISM triblock copolymer (T5) exhibiting a Q^{214} morphology, is blended with increased amounts of $PMMA_{6k}$ up to 20 vol % homopolymer content. A phase transformation from the Q^{214} to the LAM morphology occurs between blends B2 and B3.

LAM phase boundary was not a focus of this study. The following section briefly summarizes the phase assignments of the neat ISM triblock copolymers[48] and focuses on the characterization of the copolymer/homopolymer blends.

Neat ISM Triblock Copolymers. Chemical characterization (based on GPC and ^{1}H NMR) and phase assignments (based on SAXS and TEM) of seven neat ISM triblocks are reported in Table 1. Analysis of the neat triblock phase assignments can be found in a previous report,[48] with the exception of T6, which exhibits a HEX morphology. Figure 2 summarizes the SAXS patterns of the neat ISM triblocks acquired at 25 °C. In general, samples were annealed to temperatures between 200 and 250 °C prior to data acquisition. In Figure 2, the top four SAXS patterns (UD-SAXS data for triblocks T1, T2, and T4 and APS-SAXS data for triblock T3) show scattering peaks at integral spacings, characteristic of the lamellar (LAM) morphology (note: a distinction between two- and three-domain lamellae is not made for the majority of the samples in this work). The lab-source SAXS patterns of samples T1, T2, and T4 do not provide the necessary resolution to resolve clearly higher-order peaks. Therefore, unidentified, but expected, peaks are indicated by dashed arrows in all SAXS profiles presented in this work. The near absence of 3q* relative to 2q* scattering in sample T3 is suggestive of a three-domain LAM. TEM images show a layered-like structure indicative of LAM with dark PI domain and light PS/PMMA domains (not shown, except for T3 in Figure 1). APS-SAXS data obtained from T5 contain peaks consistent with the $I4_132$ space group symmetry, characteristic of the alternating gyroid (Q^{214}) morphology. UD-SAXS data for sample T6 (not previously reported) exhibit a series of diffraction peaks at q*, $\sqrt{3}$q*, $\sqrt{4}$q*, $\sqrt{7}$q*, and $\sqrt{9}$q* consistent with a hexagonally symmetry. TEM analysis of this specimen shows both perpendicularly oriented (hexagonally packed dots) and parallel stripes indicative of a hexagonally packed cylinder (HEX) morphology. Finally, UD-SAXS data from sample T7 show a broad primary peak, suggestive of a disordered melt (DIS) morphology. Additional TEM micrographs for neat triblock copolymers T3, T5, T6, and T7 are located in Figure 1. It should be noted that because OsO_4 preferentially stains the PI block the PS and PMMA domains are not easily distinguishable using TEM. However, given the relatively low segregation strengths of the neighboring blocks, we suspect that either end block of low content (PI or PMMA) can mix with the PS middle block, creating a "pseudo" two-phase morphology in samples T4 and T6 (and corresponding blended specimens, B18−B29, discussed later in this section).

Triblock Copolymer/Homopolymer Blends. Triblock copolymer/homopolymer blends were generated to refine the phase boundaries in the ISM system and to compare our system with the symmetric model ABC theoretical diagram generated by Tyler et al.[42] Blending was accomplished by adding homopolymer (Table 2) to the end block(s), middle block, or both end and middle blocks of the copolymer and transformations were noted to and from network phase regions. The results of our blending studies are provided below. (See also Table 3.)

Phase Transformations from Q^{214} Network Phase Using PMMA or PS Homopolymer. Four samples (B1−B4) were obtained by blending an alternating gyroid-forming parent triblock (T5) with increasing amounts of $PMMA_{6k}$ homopolymer up to 20 vol % PMMA. SAXS patterns of the parent and blended specimens at 25 °C are presented in Figure 3 along with a phase portrait showing the blend

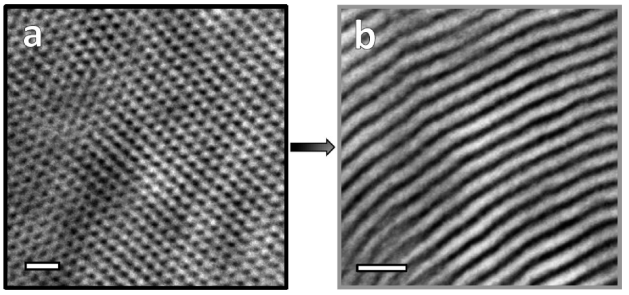

Figure 4. TEM micrographs obtained from (a) T5 and (b) blend B3. TEM images representative of the (a) Q^{214} and (b) LAM morphologies support the SAXS peak assignments. Scale bars represent 50 nm.

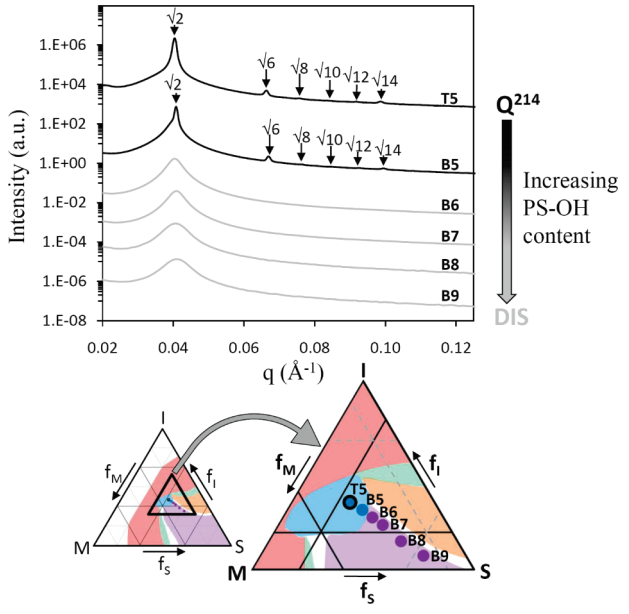

Figure 5. SAXS data for ISM triblock/PS−OH homopolymer specimens. From top to bottom: the neat Q^{214} copolymer (T5) is blended with increased amounts of $PS-OH_{9k}$ up to 24 vol % homopolymer content. A phase transformation from Q^{214} to a disordered phase (DIS) occurs between blends B5 and B6.

locations. Blends B1 and B2, containing 3 and 8 vol % PMMA homopolymer content, show similar APS-SAXS patterns with relative scattering peak positions at $\sqrt{2}q^*$, $\sqrt{6}q^*$, $\sqrt{8}q^*$, $\sqrt{10}q^*$, $\sqrt{12}q^*$, and $\sqrt{14}q^*$, where the primary peak corresponds to $\sqrt{2}q^*$. These SAXS patterns are comparable to that of the parent material T5, which exhibits an alternating gyroid (Q^{214}) morphology. Upon addition of 12 vol % PMMA homopolymer, the blended material (B3) displays a different UD-SAXS pattern with peak ratios of q*, 2q*, and 3q*, typical of LAM. TEM images support the phase transformation from Q^{214} (T5) to LAM (B3) in Figure 4a,b, respectively, where Figure 4b shows the dark layers of the PI domains and light layers of the PS and PMMA domains. Blend B4 (20 vol % PMMA homopolymer) exhibits a similar NSLS-SAXS pattern to B3 with integral ratios of scattering wave vector moduli. We believe that B3 and B4 likely exhibit a LAM_3 morphology based on the relative intensities of the diffraction peaks and relative compositions of the blocks.[12,48]

Triblock copolymer T5 was also blended with up to 24 vol % $PS-OH_{9k}$ content (B5−B9). Blend B5, containing 3 vol % PS−OH homopolymer content, exhibits the Q^{214} morphology. This assignment is supported by APS-SAXS data (Figure 5) at 25 °C that show a similar pattern to the parent T5 sample.

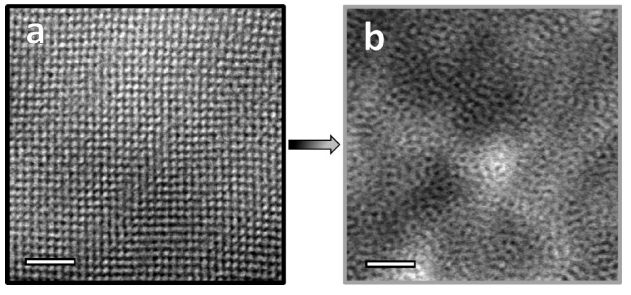

Figure 6. TEM micrographs obtained from (a) blend B5 and (b) blend B7. TEM projections are consistent with (a) a Q^{214} assignment and (b) a disordered (DIS) phase. Scale bars represent 100 nm.

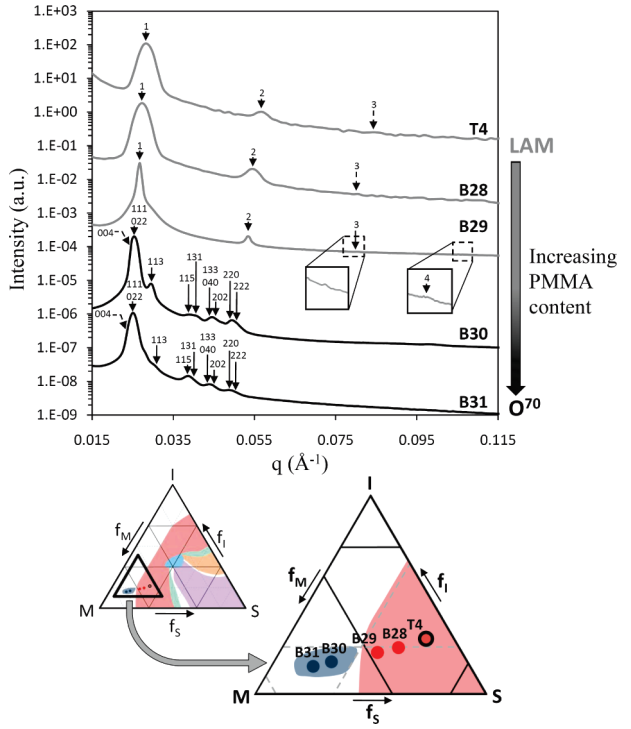

Figure 7. SAXS data for ISM triblock/PMMA blended specimens. From top to bottom: the neat LAM-forming copolymer (T4) is blended with increased amounts of $PMMA_{11k}$ up to 23 vol % homopolymer content. A LAM to O^{70} phase transformation occurs between blends B29 and B30. SAXS patterns produced from blends B30 and B31 show relative peak ratios indexed according to *Fddd* space group symmetry.

The TEM image for blend B5 (Figure 6a) is consistent with a Q^{214} assignment. Further addition of homopolymer, from 9 to 24 vol % PS−OH content, produces blends B6 through B9. SAXS patterns for these samples (APS-SAXS for B6 and B7, UD-SAXS for B8 and B9) display a single broad primary peak where the absence of higher-order peaks in these SAXS patterns suggests a disordered morphology (Figure 5). TEM micrographs show microphase separation with minimal long-range order (Figure 6b). These four blended specimens exhibit a disordered (DIS) morphology over the entire range of annealing temperatures. (See Table S1 of the Supporting Information.) It should be noted that the hydroxyl end-capping on the PS homopolymer has a minimal effect on the blending phase behavior because a PS homopolymer with no hydroxyl end-capping and molecular weight of 6700 g/mol was also used to generate a disordered blend at a comparable composition to B7. Data for this blend (not shown) indicate similar behavior and support a disordered phase assignment.

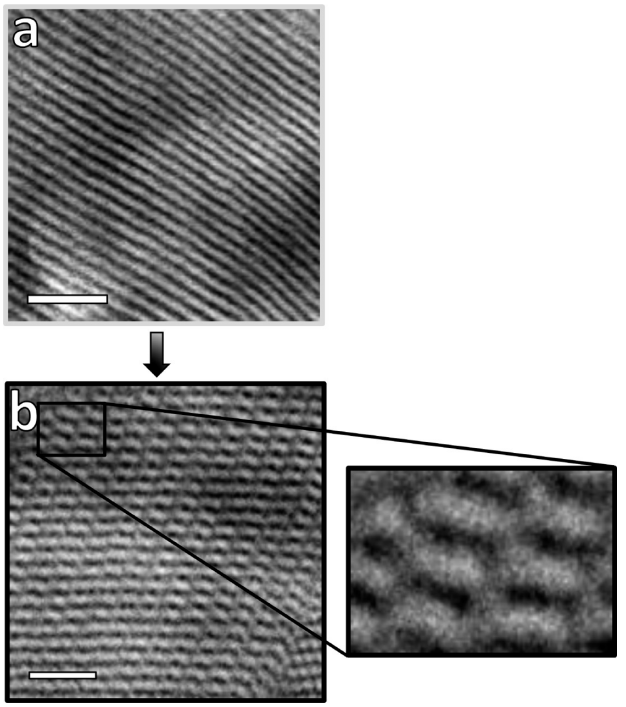

Figure 8. TEM micrographs obtained from (a) blend B28 and (b) blend B30. TEM image a is consistent with a LAM assignment, whereas TEM image b is consistent with an orthorhombic network structure where the PMMA domains are interconnected with trivalent junctions of PS domains in a dark PI matrix (emphasized in the magnified image).[12,20] Scale bars represent 100 nm.

Phase Transformations from LAM to O^{70} and Q^{230} Network Phases. A lamellae-forming triblock copolymer (T4) was blended with up to 23 vol % $PMMA_{11k}$ homopolymer. Figure 7 shows SAXS patterns obtained at 25 °C for the parent triblock T4 and corresponding blends (B28−B31). Blends B28 (UD-SAXS) and B29 (APS-SAXS), containing 6 and 10 vol % homopolymer, respectively, show diffraction peaks at q*, 2q*, and 3q* (and an additional higher-order peak located at 4q* for B29) suggestive of a LAM morphology. A TEM micrograph from B28 (Figure 8a) shows a lamellar-like morphology with thicker light stripes corresponding to the PS and PMMA domains and thinner dark stripes of the PI domains. The addition of 20 and 23 vol % PMMA homopolymer to triblock T4 produces a different SAXS signature in blends B30 (APS-SAXS) and B31 (APS-SAXS). These patterns have been indexed according to the *Fddd* space group symmetry, characteristic of the O^{70} orthorhombic network structure with lattice dimensions a/c = 0.28, b/c = 0.56, and c = 104 nm for B30 and a/c = 0.28, b/c = 0.55, and c = 106 nm for B31. TEM micrographs for B30 and B31 also support the O^{70} assignment. Figure 8b shows a TEM micrograph for blend B30, suggestive of the orthorhombic morphology with a [110] projection, where the slight ellipsoidal-shaped PMMA domains (light) are interconnected with trivalent junctions of PS in a matrix of PI domains (dark). In the work by Bailey et al. and Epps et al., schematics of the trivalent connectors in the O^{70} structure provide additional visual support of our morphological assignment.[12,20]

The LAM-forming parent triblock copolymer (T4) was also blended with increasing amounts of PS_{14k} up to 25 vol % homopolymer (B25−B27). Blends B25 and B26 with 9 and 13 vol % homopolymer, respectively, form a LAM morphology according to the indexed peak reflections obtained from APS-SAXS data (Figure 9). The LAM assignment is supported by

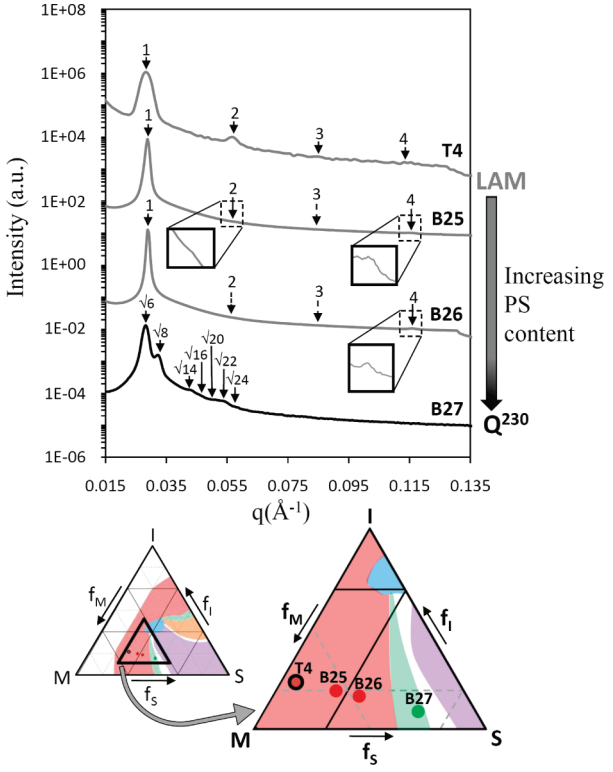

Figure 9. SAXS data for ISM triblock/PS blended specimens. From top to bottom: the neat LAM-forming copolymer (T4) is blended with increased amounts of PS_{14k} up to 25 vol % homopolymer content. A LAM to Q^{230} phase transformation occurs between blends B26 and B27.

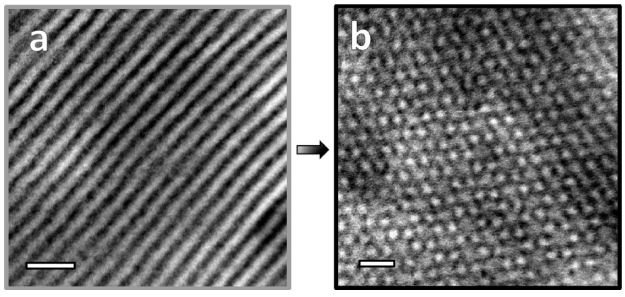

Figure 10. TEM micrographs obtained from (a) blend B25 and (b) blend B27. TEM image a is consistent with LAM, whereas TEM image b shows a "wagon-wheel" [111] projection that supports a Q^{230} assignment. Scale bars represent 50 nm.

TEM (shown for B25 in Figure 10a). Further addition of homopolymer to T4 produces a self-assembled structure described by diffraction peaks at $\sqrt{6}$q*, $\sqrt{8}$q*, $\sqrt{14}$q*, $\sqrt{16}$q*, $\sqrt{20}$q*, $\sqrt{22}$q*, and $\sqrt{24}$q* (blend B27, 25 vol % homopolymer, NSLS-SAXS), where q* = q_{112}. Although not all reflections are identifiable, this peak sequence, for which the intensity peak ratio between the first (q_{112}) and second peak (q_{022}) is roughly 10:1, is consistent with the $Ia\bar{3}d$ space group, characteristic of the Q^{230} gyroid morphology. A representative TEM micrograph of the gyroid structure with the "wagon-wheel" [111] projection (B27) is displayed in Figure 10b. Whereas PMMA and PS are indistinguishable in the TEM micrographs, we expect a core−shell gyroid morphology where channels of PMMA core domains (light) are surrounded by a thick shell of PS in a matrix of PI (dark).[12,19,52] However, we do not eliminate the possibility of PI/PS domain mixing at such low PI content in this specimen.

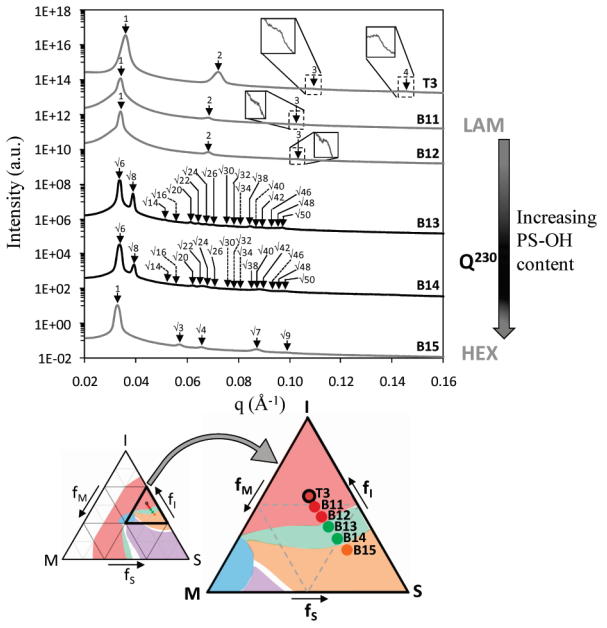

Figure 11. SAXS data for ISM triblock/PS−OH homopolymer specimens. From top to bottom: the LAM-forming triblock copolymer (T3) is blended with increasing amounts of PS−OH_{9k} up to 21 vol % homopolymer content. Phase transformations from LAM to Q^{230} to HEX occur between blends B12 and B13, and between B14 and B15, respectively.

Five blends (B11−B15) were produced from mixing another LAM-forming parent triblock (T3) with up to 21 vol % PS−OH_{9k} homopolymer. NSLS-SAXS patterns from T3 and associated blends B11 through B15 are shown in Figure 11. Blends B11 and B12, with 5 and 8 vol % homopolymer, respectively, exhibit NSLS-SAXS patterns similar to the neat triblock T3, indicative of LAM. The broadening of the first-order peak indicates a relative lack of ordering in blends B11 and B12 under the annealing conditions (Supporting Information, Table S1); however, no macrophase separation is found in either specimen. A TEM micrograph for blend B11 (Figure 12a) supports the LAM assignment. Blending T3 with 12 vol % homopolymer to produce B13 leads to a change in the self-assembled morphology. The NSLS-SAXS pattern shows high-order peak ratios that can be indexed to the $Ia\bar{3}d$ space group. (See Figure 11.) TEM analysis (Figure 12b) supports a Q^{230} assignment. The Q^{230} morphology is retained up to 16 vol % homopolymer (B14), as confirmed by NSLS-SAXS and TEM. Upon addition of 21 vol % homopolymer (B15), a different structure is found; the scattering pattern is characterized by a NSLS-SAXS pattern with reflections at q*, $\sqrt{3}$q*, $\sqrt{4}$q*, $\sqrt{7}$q*, and $\sqrt{9}$q*, consistent with a hexagonal symmetry. The TEM micrograph in Figure 12c also suggests a HEX morphology. As a result, using the same neat triblock copolymer and up to 21 vol % homopolymer addition, we show phase transformations from LAM to Q^{230} to HEX. Given the close proximity of T3 and blends B11−B15 to the IS diblock edge of the ISM triangle (low PMMA content), there exists a strong possibility for the aforementioned morphologies to exhibit "pseudo" two-domain morphologies where PMMA mixes with PS while avoiding the PI domain.

Blending within Hexagonally Packed Cylinders and from HEX to Q^{230}. To check morphological consistency between neat triblocks and blended specimens, we synthesized triblock T6 in the HEX phase region at a comparable composition to blend B15. Although the molecular weight for T6 was considerably larger ($M_{n_{T6}}/M_{n_{T3}}$ = 1.43), the HEX morphology could be identified in both samples. T6 was blended with

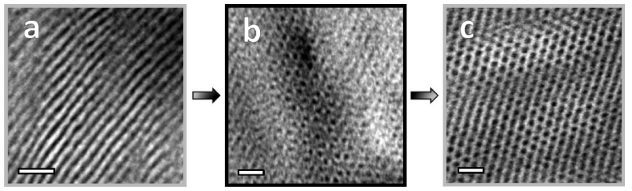

Figure 12. TEM micrographs obtained from (a) blend B11, (b) blend B13, and (c) blend B15. TEM images are consistent with (a) LAM, (b) Q^{230}, and (c) HEX assignments. Scale bars represent 100 nm.

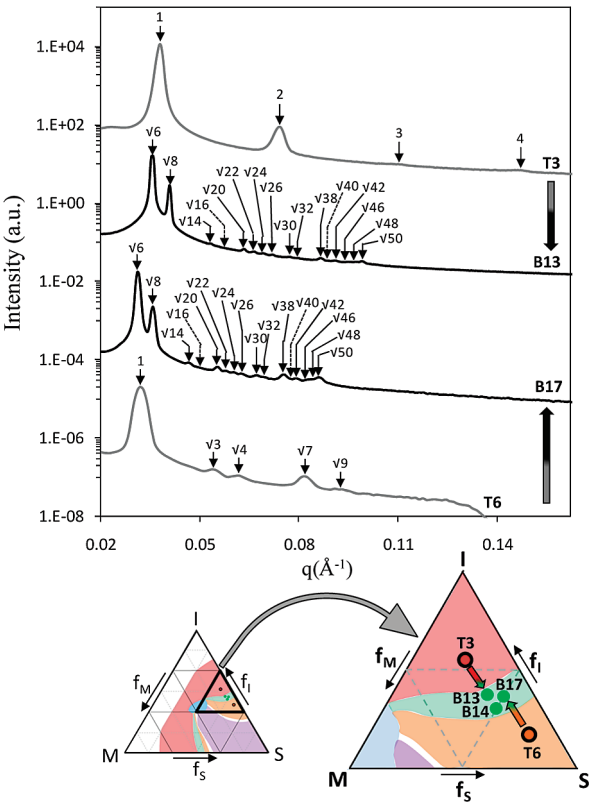

Figure 13. SAXS data shows morphological consistency between two blends B13 and B17 mixed from two different parent ISM triblocks T3 and T6, respectively. The SAXS pattern for B17 is characteristic of the double gyroid (Q^{230}) structure ($Ia\bar{3}d$ space group symmetry) and matches blend B13 of comparable composition. The difference in degree of polymerization, N = 246 for T3 and N = 338 for T6, does not alter the overall blend phase behavior in this region of the phase diagram.

various amounts of $PMMA_{1k}$ (up to 10 vol % homopolymer content) to explore the extent of the HEX region. Five ISM triblock/PMMA homopolymer blends (B18−B22) are reported in Table 3. All blended specimens exhibit the HEX morphology based on SAXS and TEM results (Supporting Information, Figures S1 and S2). Additionally, two ISM triblock/PS_{17k} homopolymer blends (B23 and B24) also exhibit a HEX structure confirmed by SAXS and TEM analysis (Supporting Information, Figures S3 and S4). Interestingly, no phase transformation from the HEX to a spherical (S) morphology is located in blends from T6 triblock and PS_{17k} up to 26 vol % homopolymer content. High homopolymer loadings (f_h > 26 vol % PS_{17k} content) were not investigated because of the potential for macroscale phase separation, and possible reasons of the absence of the sphere regions are provided in the Discussion section.

Finally, we investigated the consistency in phase behavior between two blends of comparable composition obtained from two different parent triblock copolymers. Here triblock

T6 was mixed with 6 vol % PI_{3k} homopolymer to produce B17. This sample is located in the middle of the estimated Q^{230} phase region (Figure 13), as delineated by blends B13 and B14 generated from neat triblock T3. SAXS patterns for T3 and T6 and the associated blends B13 and B17, respectively, are shown in Figure 13. The APS-SAXS pattern produced from blend B17 show a series of peak reflections similar to those found in blends B13 and B14 (Figure 11), associated with space group $Ia\bar{3}d$ and suggestive of a Q^{230} network morphology. TEM micrographs provide further support of the phase transformation from HEX (T6 in Figure 14a) to Q^{230} (B17 in Figure 14c) and from LAM (T3 in Figure 14b) to Q^{230} (B13 in Figure 14d). This blending investigation, with T3 undergoing middle-block blending and T6 undergoing end-block blending, supports morphological consistency in our blended specimens. Again, we note this blend consistency, even with the differing degrees of polymerization between T3 [parent for B13] ($N = 246$) and T6 [parent for B17] ($N = 338$).

Discussion

In this work, we present the phase behavior of neat and blended ISM triblock copolymers near the styrene-rich ISM network phase window. Whereas the analysis of neat ISM triblocks permitted the identification of LAM, HEX, DIS, and Q^{214} morphologies, judicious triblock/homopolymer blending induced phase transformations to and from network phase regions for materials with up to 26 vol % homopolymer content. This blending facilitated the identification of two additional network phase channels (Q^{230} and O^{70}) and the refinement of phase boundaries in the ISM system.

Currently, few theoretical efforts have attempted to capture the comprehensive phase behavior of ABC triblock copolymer melts.[11,36,42] With the exception of the weak-segregation theory by Erukhimovich,[53,54] the SCFT calculations by Tyler et al.[42] and the very recent complementary SCFT examinations by Qin et al.[43] are the most relevant theoretical treatments that address the morphological complexity of nonfrustrated ABC triblocks while also being directly comparable to the experimental ISM system. As stated in the Introduction, a model ISO phase diagram by Tyler et al., obtained using SCFT calculations, qualitatively matched the experimental results reported by Epps et al. and later by Chatterjee et al.;[12,15] however, several morphological discrepancies were noted such as the absence of a Q^{230} to O^{70} to Q^{214} phase progression with increasing f_S at fixed f_O. Tyler et al. also considered an idealized nonfrustrated ABC model with equal statistical segmental lengths ($b_A = b_B = b_C$) and equal segregation strengths between neighboring blocks (for $N = 250$ at 100 °C: $\chi_{AB}N = \chi_{BC}N = 13$, whereas $\chi_{AC}N = 35$).[42] This symmetric ABC model around the $f_A = f_C$ isopleth is qualitatively similar to the general morphological behavior of the ISM system because the segment lengths are close to unity ($b_M/b_I = 0.95$, $b_I/b_S = 1.11$, $b_S/b_M = 0.95$)[44] and the segregation strengths of the neighboring blocks are comparable to the χN values of the ABC model (for $N = 250$ at 100 °C: $\chi_{AB}N = \chi_{MS}N = 9.6$,[47] $\chi_{BC}N = \chi_{SI}N = 11$[46]). It should be noted that we use the notation A = M, B = S, and C = I as a matter of convention from Tyler's ABC model phase diagram, and because χ_{MS} and χ_{SI} values are nearly equal and closely dependent on temperature, the block labeling convention highly depends on the χ parameter. For the end-block interaction parameter $\chi_{AC} = \chi_{MI}$, a range of values are reported in the literature: Tcherkasskaya et al. determined χ_{MI} to be 0.077 ± 0.004 at 22 °C[45] using direct nonradiative energy transfer data, whereas Yang et al. later estimated it to be around 0.18 ± 0.02.[55] Altogether, the findings of Tcherkasskaya et al. and Yang et al. agree with the stronger segregation nature of the PI/PMMA interaction relative to the PI/PS and PS/PMMA interactions, where for $N = 250$, the end-block segregation strengths would be $\chi_{MI}N = 19 \pm 1$ and 45 ± 5, respectively.

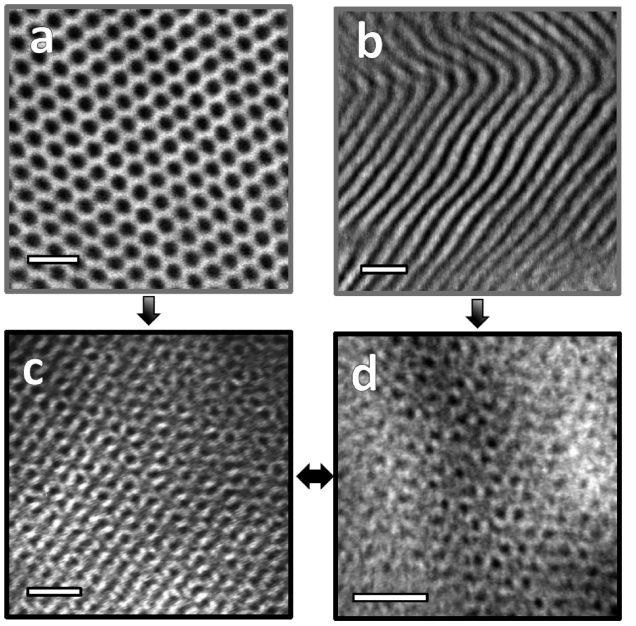

Figure 14. TEM micrographs obtained from (a) polymer T6, (b) polymer T3, (c) blend B17, and (d) blend B13. TEM projection a is consistent with HEX morphology (hexagonally packed cylinders), whereas the TEM image in b is representative of the LAM morphology. TEM micrographs in c and d correspond to the Q^{230} morphology. Scale bars represent 50 nm.

Whereas the comparison between the neat ISM materials and the ABC model phase diagram by Tyler et al. has been discussed in a previous publication,[48] minor discrepancies in the blended ISM specimens are discussed in more detail in the remainder of this section. In this work, the phase behavior of the neat and blended specimens was investigated for chains with overall degree of polymerization, ranging from roughly 150 to 340. Well-ordered double gyroid (Q^{230}) and orthorhombic (O^{70}) network structures were formed in blends of an I-lean LAM-forming material (T4: $N = 294$) with PS_{14k} homopolymer (Q^{230} found in blend B27) and with $PMMA_{11k}$ homopolymer (O^{70} found in blends B30 and B31), respectively. Additionally, the Q^{230} phase was obtained in a blend of an M-lean LAM-forming material (T3: $N = 246$) with PS homopolymer (blend B17). The locations of these LAM-to-network phase transformation sequences are reasonably consistent with the SCFT calculations of Tyler et al. However, the phase regions for the Q^{230} and O^{70} are slightly shifted in composition with respect to the model diagram. (Figure 1.) We believe that these minor discrepancies arise from the small conformational asymmetries in the ISM system that shift the phase boundary toward compositions richer in the blocks with the longer statistical segment lengths (i.e., I-rich and M-rich, respectively, in the ISM system when $b_I/b_S = 1.11$ and $b_M/b_S = 1.05$).[34] This phenomenon also occurs in the vicinity of the IS edge of the phase map, which results in "squeezed" phase regions toward the PI-richer phases and an enlarged HEX phase region (as shown by T6, B15, and B18−24).[7] Additionally, we located O^{70}-forming blends (B30 and B31) near the Q^{230}/LAM phase boundary, situated slightly above the small predicted O^{70} phase region of the ABC model. The existence of the O^{70} phase close to the SM edge of the phase triangle indicates that the O^{70} phase is possibly stable in a narrow composition window of the SM diblock phase diagram and suggests that the O^{70} structure is thermodynamically favorable in certain regions of the ISM system.[56] However, we note that the only specimens displaying

O^{70} symmetry in this report are blended materials. Although we believe that the blends likely indicate the stability of the O^{70} structure in this system, the multicomponent nature of these samples possibly explains the larger width of the orthorhombic network region relative to the SCFT calculations. The homopolymer blending can influence the curvature at the block interfaces and thus can alter the phase boundaries in the blended ISM materials. Given the addition of PMMA homopolymer with a molecular weight different from the corresponding M-block in the copolymer, a degree of polydispersity is introduced to the system. In this case, there is a tendency to curve the M/S interface toward the more polydisperse M-block phase, which could stabilize the O^{70} phase over a wider region.[57] This condition applies to all blends examined in this study because the ratio between the molecular weights of the homopolymer and that of the corresponding blocks is not strictly consistent. Therefore, the phase boundaries determined in this work are not unique but rather provide strong guidance to the true ISM phase behavior at similar segregation strengths.

Whereas the general neat and blend ISM phase behavior follows the overall morphological behavior predicted by the SCFT calculations of Tyler et al., several differences exist. The small sphere regions (S and S^A) predicted to lie on either side of the $f_A = f_C$ isopleth are not found in our ISM system within the limits of our blending study. Instead, blends of Q^{214}-forming triblock (T5) with PS−OH_{9k} homopolymer induce a phase transformation from the Q^{214} morphology directly to disordered phases (B6−B9), with no indication of the expected Q^{214} to HEX to S to DIS phase sequence. Blends of HEX-forming triblock (T6) with PS_{17k} and blends of LAM-forming triblock (T4) with PS_{14k} also showed an extensive HEX region with no evidence of spherical morphologies. We believe that packing frustration resulting from blending the copolymer S-middle-block with PS homopolymer may cause a decrease in the effective segregation strengths of the blended specimens and could destabilize a more ordered phase relative to the expected behavior of neat ISM triblocks.[21] Although we expect this phenomenon to have a minor effect given the morphological consistency of the remainder of the phase diagram, we do not eliminate the possibility that the neat ISM system can exhibit spherical morphologies. The absence of sphere regions could also be attributed to fluctuation effects given the proximity of these blends to the order-to-disorder transition regions.[58] However, the disappearance of the S and S^A phases has been recently confirmed by Qin et al. over a small range of $\chi_{AC}N$ values (and fixed $k = \chi_{AC}/\chi_{AB}$ ratios) corresponding to that of our ISM system (independently of the χ_{MI} used from literature). In this particular situation, the phase sequence of the asymmetric ABC model triblock within the AC isopleth with increasing f_B is LAM to Q^{214} to DIS, comparable to the phase sequence in the blends of Q^{214}-forming triblock (T5) with PS−OH_{9k} homopolymer.[43] This finding, by Qin et al., suggests that the value of $\chi_{AC}N$ and the ratio $k = \chi_{AC}/\chi_{AB}$ have a significant influence on the phase boundaries of a symmetric ABC copolymer, where the disappearance of spherical morphologies can occur at low enough $\chi_{AC}N$ values.

No direct evidence of the expected HEX region along the SM diblock edge of the ISM phase map was found within the limit of our blending study. We believe that this difference can be attributed to a combination of blending artifacts due to middle-block blending and slight asymmetry in the interaction parameters: as seen in the revised phase diagram for the slightly asymmetric model ISO system by Qin et al., the HEX and S regions on the left side of the AC isopleth corresponding to the most weakly segregated block interaction are significantly reduced.[43] These SCFT calculations can possibly explain the larger HEX region found along the IS edge relative to the smaller HEX region expected along the SM edge of the ISM phase map. We also note that the O^{70} network regions that neighbor the Q^{214} phase region on both sides of the $f_A = f_C$ isopleth are not found in this study. Additional neat triblock copolymers and associated blends near the Q^{214} region would be necessary to refine further the phase boundaries and locate the possible O^{70} and S^A (or S) regions predicted by the SCFT calculations.

Conclusions

The phase behavior of 7 neat ISM triblock copolymers and 31 associated ISM copolymer/homopolymer blends has been investigated in the weak-to-intermediate segregation regime near styrene-rich network regions. This experimental framework provides further insight into the understanding of the universal principles behind ABC triblock copolymers. We relied on blending techniques to access the network phase channels using triblock copolymer/homopolymer blends, where LAM, HEX, Q^{214}, Q^{230}, O^{70}, and DIS morphologies were identified in both neat and blended materials. End-block and middle-block blending of ISM triblock copolymers with constituent homopolymers was used to induce phase transformations to and from network structures. This blending technique facilitated the refinement of the phase boundaries in the vicinity of the network phase channels. Morphological consistency was confirmed between HEX-forming neat and blended specimens at similar compositions as well as between two double gyroid-forming blends, obtained from two distinct neat triblock copolymers of substantially different molecular weights and preblended compositions. In this study, the ISM phase map of neat and blended materials qualitatively matched the predicted SCFT phase behavior of a symmetric ABC model by Tyler et al. We believe that the minor discrepancies in the size and location of the phase boundaries are mainly due to a combination of small differences in the χ parameters and block statistical segment lengths between the experimental and theoretical systems and the effect of the value of $\chi_{AC}N$ and the χ_{AC}/χ_{AB} ratio. Altogether, blending appeared to have a minimal impact on the phase boundaries relative to neat ISM triblock materials. However, copolymers undergoing end-block blending with a polydisperse homopolymer possibly stabilized the O^{70} morphology near the M-rich corner of the phase map, whereas the addition of PS homopolymer to the middle block of a Q^{214}-forming copolymer possibly induced a premature destabilization of the ordered morphology leading to a Q^{214}-to-DIS phase transformation.

Acknowledgment. This work was supported by Delaware EPSCoR (EPS-0447610), NSF-NER (CBET-0707507), and NSF-CAREER (DMR-0645586). Use of the National Synchrotron Light Source, Brookhaven National Laboratory, was supported by the U.S. Department of Energy, Office of Science, Office of Basic Energy Sciences, under contract no. DE-AC02-98CH10886. Portions of this work also were performed at the DuPont-Northwestern-Dow Collaborative Access Team (DND-CAT) located at Sector 5 of the Advanced Photon Source (APS). DND-CAT is supported by E.I. DuPont de Nemours & Co., The Dow Chemical Company, and the State of Illinois. Use of the APS was supported by the U.S. Department of Energy, Office of Science, Office of Basic Energy Sciences, under contract no. DE-AC02-06CH11357. We also thank the Pochan group for some SAXS data collected at APS. We acknowledge the W. M. Keck Electron Microscopy Facility for the use of their JEOL JEM-2000FX and Tecnai-12 TEMs. Finally, we thank Nripen Singh, Elizabeth Kelley, and Sarah Mastroianni for synthesizing the PS−OH_{9k}, PS_{14k}, and PI_{3k} homopolymers used in this study.

Supporting Information Available: Detailed thermal annealing history for neat and blended specimens; SAXS patterns and TEM micrographs for seven additional blends (B18−B24)

confirm the extent of the HEX phase region along the IS diblock edge of the proposed ISM phase map. This material is available free of charge via the Internet at http://pubs.acs.org.

References and Notes

(1) Hamley, I. W. *The Physics of Block Copolymers*; Oxford Science Publications: New York, 1998.
(2) Phillip, W. A.; Amendt, M.; O'Neill, B.; Chen, L.; Hillmyer, M. A.; Cussler, E. L. *ACS Appl. Mater. Interfaces* **2009**, *1*, 472–480.
(3) Crossland, E. J. W.; Ludwigs, S.; Hillmyer, M. A.; Steiner, U. *Soft Matter* **2007**, *3*, 94–98.
(4) Lodge, T. P. *Macromol. Chem. Phys.* **2003**, *204*, 265–273.
(5) Meuler, A. J.; Hillmyer, M. A.; Bates, F. S. *Macromolecules* **2009**, *42*, 7221–7250.
(6) Bates, F. S.; Fredrickson, G. H. *Phys. Today* **1999**, *52*, 32–38.
(7) Matsen, M. W.; Bates, F. S. *J. Polym. Sci., Part B: Polym. Phys.* **1997**, *35*, 945–952.
(8) Bailey, T. S.; Pham, H. D.; Bates, F. S. *Macromolecules* **2001**, *34*, 6994–7008.
(9) Hückstädt, H.; Göpfert, A.; Abetz, V. *Polymer* **2000**, *41*, 9089–9094.
(10) Suzuki, J.; Nakane, K.; Takano, A.; Matsushita, Y. *Polymer* **2004**, *45*, 8989–8997.
(11) Tang, P.; Qiu, F.; Zhang, H.; Yang, Y. *Phys. Rev. E* **2004**, *69*, 031803.
(12) Epps, T. H., III; Cochran, E. W.; Bailey, T. S.; Waletzko, R. S.; Hardy, C. M.; Bates, F. S. *Macromolecules* **2004**, *37*, 8325–8341.
(13) Epps, T. H., III; Cochran, E. W.; Hardy, C. M.; Bailey, T. S.; Waletzko, R. S.; Bates, F. S. *Macromolecules* **2004**, *37*, 7085–7088.
(14) Epps, T. H., III; Bates, F. S. *Macromolecules* **2006**, *39*, 2676–2682.
(15) Chatterjee, J.; Jain, S.; Bates, F. S. *Macromolecules* **2007**, *40*, 2882–2896.
(16) Mogi, Y.; Nomura, M.; Kotsuji, H.; Ohnishi, K.; Matsushita, Y.; Noda, I. *Macromolecules* **1994**, *27*, 6755–6760.
(17) Sioula, S.; Hadjichristidis, N.; Thomas, E. L. *Macromolecules* **1998**, *31*, 5272–5277.
(18) Matsushita, Y.; Suzuki, J.; Seki, M. *Physica B*. **1998**, *248*, 238–242.
(19) Shefelbine, T. A.; Vigild, M. E.; Matsen, M. W.; Hajduk, D. A.; Hillmyer, M. A.; Cussler, E. L.; Bates, F. S. *J. Am. Chem. Soc*. **1999**, *121*, 8457–8465.
(20) Bailey, T. S.; Hardy, C. M.; Epps, T. H., III; Bates, F. S. *Macromolecules* **2002**, *35*, 7007–7017.
(21) Epps, T. H., III; Chatterjee, J.; Bates, F. S. *Macromolecules* **2005**, *38*, 8775–8784.
(22) Brinkmann, S.; Stadler, R.; Thomas, E. L. *Macromolecules* **1998**, *31*, 6566–6572.
(23) Bailey, T. S. *Morphological Behavior Spanning the Symmetric AB and ABC Block Copolymer States*. Ph.D. Thesis, University of Minnesota, 2001.
(24) Huang, Y.; Liu, H.; Hu, Y. *Macromol. Theory Simul.* **2006**, *15*, 321–330.
(25) Asari, T.; Matsuo, S.; Takano, A.; Matsushita, Y. *Macromolecules* **2005**, *38*, 8811–8815.
(26) Suzuki, J.; Furuya, M.; Iinuma, M.; Takano, A.; Matsushita, Y. *J. Polym. Sci., Part B: Polym. Phys.* **2002**, *40*, 1135–1141.
(27) Dotera, T. *Phys. Rev. Lett*. **2002**, *89*, 205502.
(28) Sugiyama, M.; Shefelbine, T. A.; Vigild, M. E.; Bates, F. S. *J. Phys. Chem. B* **2001**, *105*, 12448–12460.
(29) Vaidya, N. Y.; Han, C. D.; Kim, D.; Sakamoto, N.; Hashimoto, T. *Macromolecules* **2000**, *34*, 222–234.
(30) Lee, S.-H.; Char, K.; Kim, G. *Macromolecules* **2000**, *33*, 7072–7083.
(31) Lescanec, R. L.; Fetters, L. J.; Thomas, E. L. *Macromolecules* **1998**, *31*, 1680–1685.
(32) Yamaguchi, D.; Takenaka, M.; Hasegawa, H.; Hashimoto, T. *Macromolecules* **2001**, *34*, 1707–1719.
(33) Matsen, M. W. *Macromolecules* **1995**, *28*, 5765–5773.
(34) Matsen, M. W.; Bates, F. S. *Macromolecules* **1995**, *28*, 7298–7300.
(35) Kou, D.; Jiang, Y.; Liang, H. *J. Phys. Chem. B* **2006**, *110*, 23557–23563.
(36) Fredrickson, G. H.; Bates, F. S. *Eur. Phys. J. B* **1998**, *1*, 71–76.
(37) Bosse, A.; Tirumala, V. R.; Lin, E. K. *J. Polym. Sci., Part B: Polym. Phys*. **2009**, *47*, 2083–2090.
(38) Winey, K. I.; Thomas, E. L.; Fetters, L. J. *Macromolecules* **1991**, *24*, 6182–6188.
(39) Winey, K. I.; Thomas, E. L.; Fetters, L. J. *Macromolecules* **1992**, *25*, 2645–2650.
(40) Hashimoto, T.; Tanaka, H.; Hasegawa, H. *Macromolecules* **1990**, *23*, 4378–4386.
(41) Hashimoto, T.; Yamasaki, K.; Koizumi, S.; Hasegawa, H. *Macromolecules* **1993**, *26*, 2895–2904.
(42) Tyler, C. A.; Qin, J.; Bates, F. S.; Morse, D. C. *Macromolecules* **2007**, *40*, 4654–4668.
(43) Qin, J.; Bates, F. S.; Morse, D. C. *Macromolecules* **2010**, *43*, 5128–5136.
(44) Fetters, L. J.; Lohse, D. J.; Richter, D.; Witten, T. A.; Zirkel, A. *Macromolecules* **1994**, *27*, 4639–4647.
(45) Tcherkasskaya, O.; Ni, S.; Winnik, M. A. *Macromolecules* **1996**, *29*, 610–616.
(46) Hanley, K. J.; Lodge, T. P. *J. Polym. Sci., Part B: Polym. Phys.* **1998**, *36*, 3101–3113.
(47) Russell, T. P.; Hjelm, R. P.; Seeger, P. A. *Macromolecules* **1990**, *23*, 890–893.
(48) Tureau, M. S.; Epps, T. H., III. *Macromol. Rapid Commun*. **2009**, *30*, 1751–1755.
(49) Allen, R. D.; Long, T. E.; McGrath, J. E. *Polym. Bull*. **1986**, *15*, 127.
(50) Varshney, S. K.; Jacobs, C.; Hautekeer, J. P.; Bayard, P.; Jerome, R.; Fayt, R.; Teyssie, P. *Macromolecules* **1991**, *24*, 4997–5000.
(51) Hillmyer, M. A.; Bates, F. S. *Macromolecules* **1996**, *29*, 6994–7002.
(52) Avgeropoulos, A.; Dair, B. J.; Hadjichristidis, N.; Thomas, E. L. *Macromolecules* **1997**, *30*, 5634–5642.
(53) Erukhimovich, I. Y.; Abetz, V.; Stadler, R. *Macromolecules* **1997**, *30*, 7435–7443.
(54) Erukhimovich, I. Y. *Eur. Phys. J. E* **2005**, *18*, 383–406.
(55) Yang, J.; Lu, J.; Rharbi, Y.; Cao, L.; Winnik, M. A.; Zhang, Y.; Wiesner, U. B. *Macromolecules* **2003**, *36*, 4485–4491.
(56) Kim, M. I.; Wakada, T.; Akasaka, S.; Nishitsuji, S.; Saijo, K.; Hasegawa, H.; Ito, K.; Takenaka, M. *Macromolecules* **2009**, *42*, 5266–5271.
(57) Meuler, A. J.; Ellison, C. J.; Evans, C. M.; Hillmyer, M. A.; Bates, F. S. *Macromolecules* **2007**, *40*, 7072–7074.
(58) Bates, F. S.; Fredrickson, G. H. *Annu. Rev. Phys. Chem*. **1990**, *41*, 525–557.